Image completion by diffusion maps and spectral relaxation

Shai Gepshtein,* Yosi Keller†

Abstract

We present a framework for image inpainting based on the Diffusion Framework. By choosing appropriate diffusions kernels and image affinity measures, the corresponding Diffusion embedding is shown to be smoother than the source image and can thus be inpainted by simple exemplar-based and variational methods. We discuss the properties of the induced smoothness and relate it to the underlying assumptions used by previous inpainting schemes. As the Diffusion embedding in non-linear and non-invertible, we propose a novel computational approach to computing an approximate mapping from the embedding space to the image domain. We formulate the mapping as a discrete optimization problem, solved via spectral relaxation. As the embedding space provides a canonical smooth representation, our approach can inpaint both textured and smooth images. The effectiveness of the presented method is exemplified by inpainting real images, and comparisons to previous state-of-the-art schemes.

1 Introduction

Image inpainting algorithms aim to fill the missing data of an image or a video sequence in a visually plausible way, such that the insertion is not easily detectable by a common unsuspecting viewer. Thus, this problem lies at the intersection of computer graphics, image, and signal processing. Formally, given a corrupted image I and a "hole" region mask H marking the unknown area, the goal of image completion is to fill in H to form a visually plausible image $\hat{I}$. This is depicted in Fig. 1a.

The problem has attracted significant research effort, and existing methods can be categorized as being either exemplar-based or variational schemes. Variational schemes [1, 2, 3, 4] formulate the

*Faculty of Engineering, Bar Ilan University, Israel. shaigep@gmail.com.

†Faculty of Engineering, Bar Ilan University, Israel. yosi.keller@gmail.com.

inpainting as the minimization of a variational functional that encodes spatial smoothness constraints. The minimizations of such functionals results in the solution of linear or nonlinear heat equations. Thus, these schemes assume that the inpainted images contain piecewise smooth spatial manifolds. Exemplar-based schemes [5, 6, 7, 8] implicitly assume that H can be inpainted by replicating image patches given in a reference set $\overline{H}$, that might consist of the known parts of the input image $I = \overline{H} \cup H$, or a given set of images [9, 10]. Such schemes were proven to provide efficient solutions, but lack the global optimality of the variational approaches. A combination of these two classes of methods were also proposed utilizing both global geometric completion and texture synthesis [11, 12].

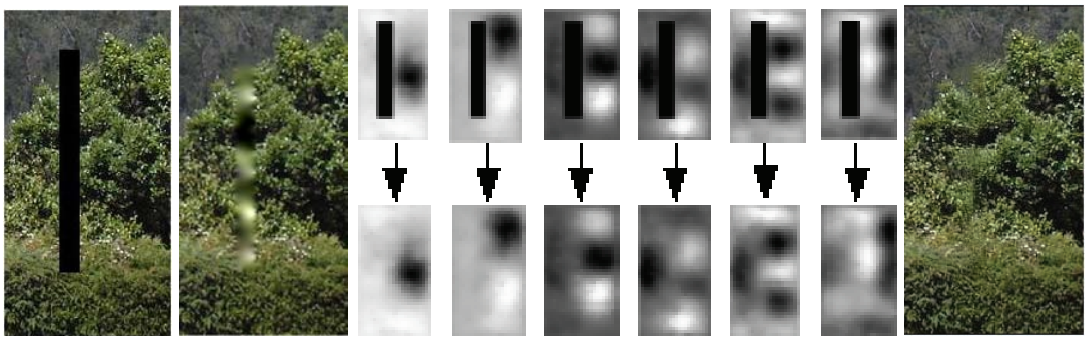

(a) (b) (c) (d)

Figure 1: (a) Source image to be inpainted. (b) The source image inpainted by an isotropic heat equation. (c) The leading eigenvectors inpainted using an isotropic heat equation (d) The image inpainted by computing the inverse Diffusion mapping of (c).

In this work, we propose a new image inpainting framework where the completion algorithm is executed in a diffusion map feature space [13]. Each pixel $\mathbf{x}_{ij} \in I$ in the reference set $\overline{H}$ is represented by a patch $\mathbf{p}_{ij} \in \mathbb{R}^D$, thus forming the reference set $\{\mathbf{p}_{ij}\}$, where D is typically 5×5 or 7×7. To analyze this high dimensional data set, we use diffusion maps for dimensionality reduction. Thus, we implicitly assume that the unknown image patches $\mathbf{p}_{ij} \in H$ and the patches in the reference set $\mathbf{p}_{ij} \in \overline{H}$ belong to the same low dimensional manifold, parameterized by the diffusion kernel. The dimensionality reduction is feasible due to the low intrinsic dimensionality of the image patches, manifested by their local correlations [14]. Using the embeddings, patches are mapped into a low dimensional space

$$\overline{H} \longmapsto \Psi(\overline{H}), \Psi \in \mathbb{R}^d,\ d << D \tag{1}$$

This is shown in Fig. 1, where a textured image contains a rectangular hole H to be filled. Applying

a variational inpainting scheme might result in excessive smoothing (Fig. 1b). However, using diffusion maps to reduce the dimensionality of the data, the resulting embedding (eigenvectors) shown in Fig. 1c, is smooth. Due to this smoothness, the holes in the 'images' of the eigenvectors can be inpainted using simple interpolation methods. As the Diffusion embedding is nonlinear, and non-invertible, the missing data in the image domain cannot be computed directly. For that, we derive a novel approximate embedding inversion scheme that assigns an image patch $\mathbf{p}_{ij} \in \overline{H}$ to each inpainted point $\mathbf{y}_{ij} \in \left\{\psi_{k_1}(\mathbf{x}_{i,j})...\psi_{k_m}(\mathbf{x}_{i,j})\right\}^T$ in the embedding domain. The assignment problem is solved via spectral relaxation [15] and induces spatial regularization.

Thus, we provide two core contributions: **First**, a general framework for data completion by deriving smooth representations via Diffusion embedding. In particular, it provides a unified scheme to inpainting textured and textureless images. **Second**, we derive a scheme for approximating the inverse of the Diffusion embedding and map the interpolated embeddings back to the data/image domain, by formulating the inverse-mapping as an assignment problem, that optimizes a global smoothness constraint. The solution to the resulting combinatorial problem is NP-hard, and is efficiently approximated by spectral relaxation.

The framework we present is general in nature and can be applied to many data sources of interest such as audio signals and tabular data. Yet, in this work we chose to concentrate on the image inpainting problem that provides an intuitive testbed for data embedding and a baseline of previous state-of-the-art works to compare against.

This paper is organized as follows: we start by reviewing previous works on image inpainting in Section 2.1 and recalling the diffusion framework in Section 2.2. The proposed image inpainting schemes is introduced and discussed in Section 3. It is experimentally verified and compared with existing approaches in Section 4. Concluding remarks are discussed in Section 5.

2 Background

In this section we survey previous results in image inpainting (Section 2.1) and provide background on the Diffusion Maps (Section 2.2) that is the main computational tool used in our work.

2.1 Image inpainting

The study of image inpainting lies at the intersection of image processing and computer graphics. Thus, the fundamentals of many contemporary inpainting schemes can be traced back to the seminal contributions of Efros and Leung [5] (exemplar-based) and Bertalmío [1] *et al.* (variational schemes).

Exemplar based techniques proved to be successful in dealing with large-scale image completion tasks (note the *Bungee* example in Fig. 14). Such methods fill the missing pixels by copying source patches from the observed part of the image to produce plausible visual results. Texture synthesis by non-parametric sampling was first introduced by Efros and Leung [5] that proposed a greedy scheme that operates on the pixels of the boundary ∂H, and successively fills the hole towards its center. The most similar patch (in terms of the L_2 norm) in I is found and copied as the predicted new value. Such schemes are sensitive to the filling order, and might propagate errors of wrongly selected filling pixels, leading to visual inconsistencies.

Criminisi *et al.* [6] extended the previous scheme by introducing priority ordering to derive the order in which the pixels are synthesized. The ordering is given by two terms. The first quantifies the strength of the isophotes hitting the hole's border, thus encouraging linear structures with high strength of isophotes to be synthesized first. The second encodes the reliability of the information in the pixel's vicinity. Therefore, patches that have more of their neighboring pixels already filled will be filled first. The priority assignment is a product of the two terms computed at each pixel and updated in each iteration of the algorithm.

A globally optimal formulation of exemplar based inpainting was suggested by Wexler *et al.* [7], where the objective function adds a constraint that missing pixels have to be consistent with all the surrounding patches forming them. In order to reach a global optimum, the inpainting is iterated until the update converges. This approach utilizes a multi-scale formulation by initiating the iterative completion at the coarsest level of the pyramid, and propagating the result upward. This allows improved global consistency and speeds up the convergence. The authors extended this approach [7] by introducing spatial and temporal constraints for video inpainting via a variational formulation.

Another iterative exemplar based scheme was suggested by Drori *et al.* [8], where the unknown region is approximated by classifying the pixels to an underlying structure that agrees with other parts of the image. The approximated region is then augmented with details extracted from high confidence

regions. The scheme is iterated in different scales until convergence.

The computational bottleneck of exemplar-based schemes is the search for the patch most similar to the one being inpainted, as this search is repeated at each iteration. Barnes *et al.* [16] proposed an efficient approach to K-nn search of image patches, denoted as Patchmatch that provides an order of magnitude performance improvement over previous state-of-the-art schemes such as KD-trees. Their approach is based on random initiation of the patch matches followed by the propagation of patches in the vicinity of well matched patches. It was successfully applied to applications such as image inpainting, retargeting and reshuffling.

The focal point of variational schemes is to formulate the inpainting problem as the minimization of variational functionals. Using the calculus of variations, the minimization of such functionals boils down to the solution of a nonlinear PDEs [1], where the pixels on the boundary ∂H, are used as boundary conditions. Thus, image information is propagated from ∂H into the hole H. The propagation is governed by the chosen functional and the resulting PDE, where nonlinear anisotropic diffusion is preferred to isotropic diffusion as it avoids over smoothing. Some schemes [2, 17] propose to directly choose a PDE with desirable inpainting properties, without deriving it by the minimization of a functional and are thus non-variational. Such schemes were shown to be beneficial when inpainting piecewise smooth images or when the hole H is relatively narrow. Yet, they might fail when inpainting the textured parts of an image.

One of the first schemes utilizing the propagation approach was suggested by Masnou *et al.* [18], that inpaint by joining points of level lines arriving at the boundary of H with geodesic curves. The edges recovered by this approach are smooth and continuous at the boundary of the hole, and it shows good results for inpainting thin holes. A combination of variational and exemplar based methods was proposed by Bertalmio [12] and Bugeau [11]. The algorithm combines texture synthesis and geometric methods for image inpainting through structure-texture decomposition. Bugeau [11] applied PDE-based techniques to the structure image that is smoother than the original one, and encodes the high frequencies of the image.

Tschumperle and Deriche [17] proposed a general framework for vector-valued image regularization, that is based on variational methods and PDEs. They derive local filters based on anisotropic diffusion. The approach is shown to be applicable to a class of image processing tasks such as image

magnification, restoration and inpainting. An image inpainting scheme that combines exemplar-based and PDE-based approaches was suggested by Le Meur *et al.* [19]. The structure tensor is used to set the filling order in the isophote direction, while the optimal image patch used to inpaint the hole, is found via template matching.

An inpainting scheme based on discrete optimization was suggested by Komodakis *et al.* [20], where a discrete variational-like functional is iteratively minimized using priority-belief propagation. The scheme solves a global discrete optimization over all possible patches, using dynamic label-pruning to significantly reduce the number of labels. A different class of recent results is based on sparse reconstruction [21, 22], where an image is represented as a set of image patches that are processed as a set of high dimensional samples for which a sparse dictionary is learnt. The missing data H is extrapolated by linear combinations of the dictionary atoms, computed via L_1 minimization.

Our work relates to both variational and sparse reconstruction based approaches, as these assume that the inpainted image belongs to a low-dimensional space, being either the space of smooth images (as in the variational approaches) or in the space spanned by a sparse dictionary. Our scheme utilizes a different notion of low dimensionality and smoothness that relates to the Diffusion Framework [13]. By utilizing application-specific affinity measures and kernels (Section 3.3) we *induce* a chosen smoothness over the image manifold. Thus, simple variational approaches can be applied to inpaint textured images. These different notions of smoothness are further discussed in Section 3.4.

2.2 Diffusion maps

In this Section we survey the diffusion framework, where a broader view can be found in [13, 14]. Given a set $X = \{\mathbf{x}_1, ..., \mathbf{x}_n\}$ of n data points, such that $\mathbf{x}_i \in \mathbb{R}^D$. Our goal is to compute a set $Y = \{\mathbf{y}_1, ..., \mathbf{y}_n\}$, where $\mathbf{y}_i \in \mathbb{R}^d$, such that $\mathbf{y}_i$ represent $\mathbf{x}_i$. Such representation forms a low dimensional mapping of the data points if $d \ll D$.

The core of the Diffusion framework is to represent the input dataset X by an undirected graph $G = (V, E)$ with nodes $V = \{\mathbf{x}_1, ..., \mathbf{x}_n\}$, and edges that quantify the affinity between two "close" points $\mathbf{x}_i$ and $\mathbf{x}_j$, such that $E \in w_{i,j}$. The affinity $w_{i,j}$ is required to be symmetric, non-negative and is commonly computed using a RBF kernel

$$w_{i,j} = \exp(-\|\mathbf{x}_i - \mathbf{x}_j\|^2/\sigma^2) = \exp(-{d_{ij}}^2/\sigma^2) \tag{2}$$

where $\sigma > 0$ is a scale parameter. σ is a measure of closeness that may prune edges from the graph such that two points $\mathbf{x}_i$ and $\mathbf{x}_j$ will have nonzero affinity $w_{i,j}$ if their distance $d_{ij} < 3\sigma$. This weight is related to the heat kernel and defines the nearest neighbor structures of the graph.

The computation of $w_{i,j}$ is application-specific. In images, the distance d_{ij} is chosen to encode different image attributes such as color spaces (RGB, LAB), texture via texture descriptors (such as LBP), and low-level image structures (edges). This is further discussed in the context of our work in Section 3.3. Coifman and Lafon [13] proved that *any* weight of the form $h(\|\mathbf{x}_i - \mathbf{x}_j\|)$ allows to approximate the heat kernel if h decays sufficiently fast at infinity, and this justifies the use of the RBF kernel in Eq. 2. The core of the diffusion framework is to induce a random walk on the data set X by normalizing the weights to a Markov matrix

$$\mathbf{A} = \mathbf{D}^{-1}\mathbf{W} \tag{3}$$

where $d_{ii} = \sum_j w_{i,j}$ is the degree of node $\mathbf{x}_i$. $\mathbf{A}$ is row stochastic and can be viewed as a random walk process as $a_{i,j} \geq 0$ and $\sum_j a_{i,j} = 1$. The term $a_{i,j}$ represents the probability to jump from $\mathbf{x}_i$ to $\mathbf{x}_j$ in a single time step. The corresponding matrix $\mathbf{A} \in \mathbb{R}^{n \times n}$ represents the transitions of this Markov chain in a single step

$$a_{ik}^t = Pr(x(t) = \mathbf{x}_k \mid x(0) = \mathbf{x}_i). \tag{4}$$

$\mathbf{A}$ encodes a time-homogeneous Markov chain, and taking powers of this matrix amounts to running the chain forward in time. $\mathbf{A}^t$ represents the probabilities of transition from $\mathbf{x}_i$ to $\mathbf{x}_j$ in t time steps. If the graph is connected, the stationary distribution that satisfies the equation $\phi_0^T \mathbf{A} = \phi_0^T$ is also the left eigenvector of the transition matrix $\mathbf{A}$ associated with the eigenvalue $\lambda_0 = 1$.

The observation of the weights as probabilities of a random walk process paves the way for a spectral decomposition scheme. The eigendecomposition of the transition matrix with respect to the Markovian time variable t yields

$$\mathbf{A}^t(x_i, x_j) = \sum_{l \geq 0} \lambda_l^t \psi_l(\mathbf{x}_i) \phi_l(\mathbf{x}_j), \tag{5}$$

where $\{\lambda_l\}$ is the sequence of eigenvalues of $\mathbf{A}$ (with $\lambda_0 = 1$) and $\{\phi_l\}$ and $\{\psi_l\}$ are the corresponding biorthogonal left and right eigenvectors. Due to the spectrum decay, only a few terms are needed to achieve a given relative accuracy in Eq. 5.

The diffusion distance quantifies the similarity between two points $\mathbf{x}_i$ and $\mathbf{x}_j$ by their probability distributions

$$D_t^2(\mathbf{x}_i, \mathbf{x}_j) = \sum_{k \in \Omega} \frac{(a_{ik}^t - a_{jk}^t)^2}{\phi_0(k)}. \tag{6}$$

This quantity is a weighted L_2 distance between the conditional probabilities a_{ik}^t and a_{jk}^t, that can be thought of as features measuring the interaction of the nodes $\mathbf{x}_i$ and $\mathbf{x}_j$ with the rest of the graph. The relation between the diffusion distance and the eigenvectors is given by

$$D_t^2(\mathbf{x}_i, \mathbf{x}_j) = \sum_{l \geq 1} \lambda_l^{2t} (\psi_l(\mathbf{x}_i) - \psi_l(\mathbf{x}_j))^2 \tag{7}$$

This identity implies that the right eigenvectors can be used to compute the diffusion distance, where the different eigenvectors are weighted by the corresponding eigenvalues $\{\lambda_l\}$, and only a few terms are needed to achieve a given relative accuracy in Eq. 7 due to the spectrum decay.

Hence, the right eigenvectors $\{\psi_l\}$ can be used as a new set of coordinates for the set X, such that the Euclidean distance between these Diffusion coordinates $\{\psi_l\}$ approximates the diffusion distance in Eq. 7. Let $d(t)$ be the number of terms retained, the *diffusion map* (embedding) is given by

$$\Psi_t : \mathbf{x} \longmapsto \left(\lambda_1^t \psi_1(\mathbf{x}), \lambda_2^t \psi_2(\mathbf{x}), \ldots, \lambda_{d(t)}^t \psi_{d(t)}(\mathbf{x}) \right)^T. \tag{8}$$

Using the diffusion map, we represent a graph of any generic data set as a cloud of points in a Euclidean space, where the chosen affinity measure allows to quantify a particular, application-specific distance measure.

3 Image completion

Let I be an image consisting of an unknown part H and its complementary $\overline{H}$, and let ∂H be the boundary of H. We aim to inpaint H by extending the boundary values $I(\partial H)$ into H, as depicted in Fig. 2.

The core of our approach is to represent the image in the Diffusion space discussed in Section 2.2, and inpaint the embedding, instead of inpainting the pixel values as in previous works. By choosing an appropriate similarity measure between the pixels $\mathbf{x}_i \in \overline{H}$, the embedding can be made smooth, thus allowing simple inpainting in the Diffusion domain. The spatial smoothness of the embedding vectors stems from them being the eigenvectors of a Sturm–Liouville operator, where similar to the Fourier domain, the leading eigenvector is the smoothest, constant vector, and the following eigenvectors become

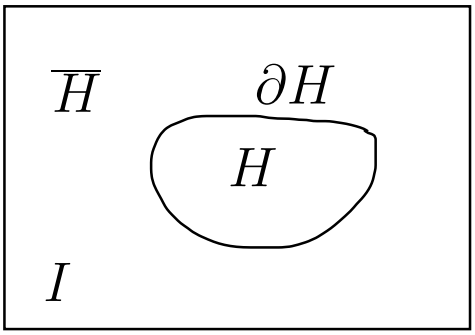

Figure 2: The image completion problem. We are given an image I, the unknown part H and its complementary $\overline{H}$, such that $I = H \cup \overline{H}$. ∂H is the boundary of H.

successively oscillatory, analogue to the higher frequencies in the Fourier domain. This is exemplified in Fig. 1c.

$\overline{H}$, the known part of the image, is used as a learning set to compute the embedding of the image manifold. In general, $\overline{H}$ can be any set of image features, for instance, $\overline{H}$ can be extracted from a video sequence [7] or a large dataset of images [9]. Following Section 2.2, each pixel $\mathbf{x}_{i,j} \in \overline{H}$ is mapped to a d dimensional Diffusion embedding space

$$\Psi : \mathbf{x}_{i,j} \longmapsto (\lambda_1 \psi_1(\mathbf{x}_{i,j}), \lambda_2 \psi_2(\mathbf{x}_{i,j}), \ldots, \lambda_d \psi_d(\mathbf{x}_{i,j}))^T \tag{9}$$

This mapping provides d eigenvectors $\{\psi_i(\mathbf{x}_{i,j})\}_1^d$ forming a d-dimensional manifold where 'similar' pixels in the image domain are mapped to close locations on the manifold. The notion of similarity is set by the particular choice of the feature space used to compute the embedding Ψ, and it is common to represent a pixel $\mathbf{x}_{i,j} \in I$ by an image patch $\mathbf{p}_{i,j} \in I$, centered at (i, j). The patch-based representation allows to characterize the image texture as discussed in Section 3.3. The dimensionality of the embedding space, (the number of eigenvectors used), is related to the intrinsic dimensionality of the image.

The smoothness of the resulting embeddings is exemplified in Fig. 3, where a textured image is embedded using the LBP texture descriptor [23] as an affinity measure that quantifies texture similarity. Thus, although the image is discontinuous in the image domain, patches with similar texture are closely mapped.

Given the embedding $\Psi \in \mathbb{R}^d$ of the set $\overline{H}$ we aim to inpaint/extrapolate Ψ onto H. For that one can apply any inpainting/interpolation scheme to the embedding vectors. To exemplify the validity of our

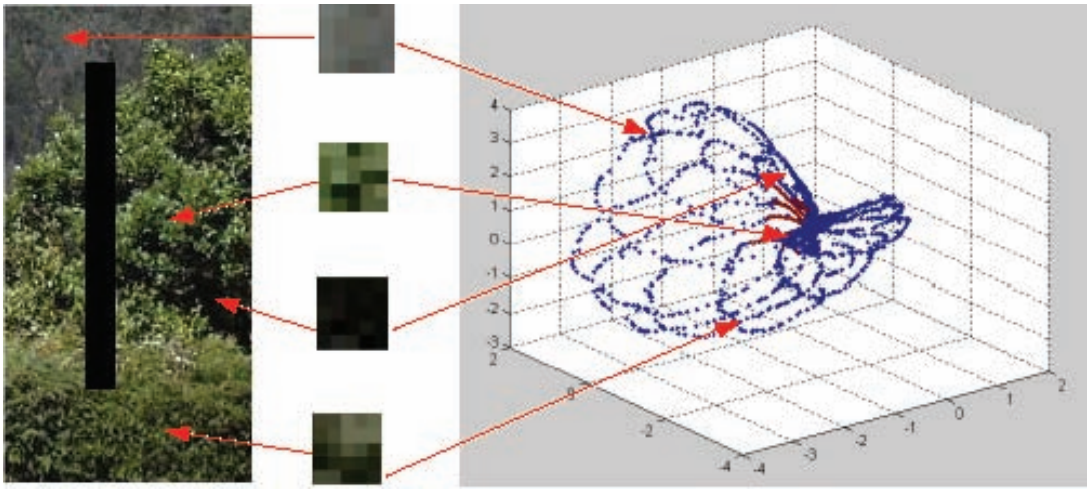

Figure 3: An image and its embedding. Patches with similar texture are mapped to close locations on the manifold, using an embedding based on LBP texture descriptors [23].

approach, we chose to use a simple linear isotropic diffusion

$$\triangle\varphi_i = 0,\ \varphi_i(\partial H) = \psi_i(\partial H)\,.\ i = 1..d \tag{10}$$

Equation 10 is applied to each eigenvector ψ_i separately, and while this approach is inferior to using multidimensional nonlinear variational schemes, it emphasizes the simplicity of the inpainting problem, as formulated in the embedding domain. We also applied Criminisi's exemplar based approach [6] in the embedding domain to compare against the isotropic interpolation.

Having computed the extrapolated embedding coordinates $\{\varphi_i(\mathbf{x}_{i,j})\}_1^d$ defined over H, we aim to relate the embedding coordinates to pixel values in the image domain. Thus, each inpainted pixel $\mathbf{x}_{i,j} \in H$ is represented by its diffusion coordinates $\mathbf{y}_{i,j} \in \mathbb{R}^d$. Unfortunately, the Diffusion embedding is nonlinear and non-invertible. Thus, the mapping $\Psi^{-1} : \mathbf{y}_{i,j} \longmapsto \mathbf{x}_{i,j}$ is non-analytic and should be approximated numerically. For that we retain for each inpainted point $\mathbf{y}_{i,j} \in \mathbb{R}^d$ its K nearest neighbors $Z_{i,j} = \left\{\mathbf{y}_{i,j}^1, ..., \mathbf{y}_{i,j}^K\right\} \in \mathbb{R}^d$ in terms of diffusion coordinates, that correspond to the set of patches $\widehat{\mathbf{p}}_{i,j} = \left\{\mathbf{p}_{i,j}^1, ..., \mathbf{p}_{i,j}^K\right\}$.

3.1 Approximate diffusion mapping inversion

In order to solve for the best patch candidates that would allow a globally optimal solution, we aim to assign each image location (i, j) to one of the potential K matches $\widehat{p}_{i,j}$. The pairwise matching potentials

quantify the spatial smoothness between neighboring patches inside of H, while enforcing consistency with the pixels on the boundary ∂H.

Given the set of $\left\{\mathbf{p}_{i,j}^{k}\right\}_{1}^{K}$ assignments per inpainted pixel $\mathbf{x}_{i,j} \in H$, we formulate a discrete variational approach for choosing the optimal inpainted image values. The discrete formulation, where a single patch $\mathbf{p}_{i,j}^{*}$ will be fit to each pixel $\mathbf{x}_{i,j}$, allows to overcome the over-smoothing effect when inpainting textured images using linear combinations of image patches. For that we induce smoothness in the image domain by minimizing the discrepancies between overlapping image patches

$$\left\{\mathbf{p}_{i,j}^{*}\right\} = \arg\min_{\mathbf{p}_{i,j}} \sum_{i,j} \sum_{k_1,k_2=-1}^{1} \left\|\mathbf{p}_{i,j} - \mathbf{p}_{i+k_1,j+k_2}\right\|^2, \quad \text{s.t. } \mathbf{p}_{i,j} \in \left\{\mathbf{p}_{i,j}^{k}\right\}_{1}^{K} \tag{11}$$

Equation 11 implies that for each image location (i, j) we aim to choose a patch $\mathbf{p}_{i,j}^{*}$ out of the K possible patches $\widehat{p}_{i,j} = \left\{\mathbf{p}_{i,j}^{1}, ..., \mathbf{p}_{i,j}^{K}\right\}$, such that the overall discrepancy over the hole H is minimized. This is a pairwise assignment problem that can be formulated as

$$\mathbf{v}^{*} = \arg\max_{\mathbf{v}} \mathbf{v}^{T}\mathbf{C}\mathbf{v}, \mathbf{v} \in \{0,1\}^{|H|K} \tag{12}$$

where $|H|$ is the number of (unknown) pixels in H. $\mathbf{v}$ is a row vectorized replica of the assignment matrix $\mathbf{V} \in \{0,1\}^{|H|\times K}$ such that $v_{i,j} = 1$ implies that the location i corresponds to the j'th patch in $\widehat{\mathbf{p}}_{i,j}$. The pairwise assignment weight matrix $\mathbf{C}$ is computed such that

$$c_{((i-1)k+j),((i'-1)k+j')} = \exp -\Delta\left(\mathbf{p}_{i,j} - \mathbf{p}_{i\prime,j\prime}\right)/\sigma^2. \tag{13}$$

where $\Delta\left(\mathbf{p}_{i,j} - \mathbf{p}_{i\prime,j\prime}\right)$ is the normalized sum of square differences (SSD) between the common support of the patches shown in Fig. 4. $\Delta\left(\mathbf{p}_{i,j} - \mathbf{p}_{i\prime,j\prime}\right)$ is computed by

$$\Delta\left(\mathbf{p}_{i,j} - \mathbf{p}_{i\prime,j\prime}\right) = \sum_{k_1,k_2 \in \mathbf{p}_{i,j} \cap \mathbf{p}_{i\prime,j\prime}} \frac{\left(\mathbf{p}_{i+k_1,j+k_2} - \mathbf{p}_{i\prime+k_1,j\prime+k_2}\right)^2}{\left|\mathbf{p}_{i,j} \cap \mathbf{p}_{i\prime,j\prime}\right|}, \tag{14}$$

where $\left|\mathbf{p}_{i,j} \cap \mathbf{p}_{i\prime,j\prime}\right|$ is the area of the common support.

Note that we replaced the minimization in Eq. 11 with the maximization in Eq. 12, which allows to weigh down the numerical effect of outlier assignments that might dominate the formulation in Eq. 11.

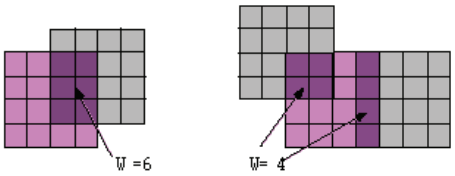

Figure 4: The normalzed discrepancy between the overlapping patches $\mathbf{p}_{i,j}$ and $\mathbf{p}_{i',j'}$. We compute the sum of square differences (SSD) over the common support $\mathbf{p}_{i,j} \cap \mathbf{p}_{i',j'}$, and normalize by its area $\left|\mathbf{p}_{i,j} \cap \mathbf{p}_{i',j'}\right|$.

Given the solution of Eq. 12, we paste the chosen candidates at the corresponding missing pixels in H. As patches overlap, the overlapping pixels are blending by averaging.

Optimizing Eq. 12 is denoted as the *Quadratic Assignment Problem* (QAP) that is known to be *NP*-hard. Hence, the exact inference of the assignments is intractable and we resort to a suboptimal solution based on spectral relaxation, where we relax the discrete optimization problem in Eq. 12, to an optimization problem with respect to a continuous variable $\mathbf{w}$

$$\mathbf{w}^* = \arg\max_{\mathbf{w}} \frac{\mathbf{w}^T \mathbf{A} \mathbf{w}}{\mathbf{w}^T \mathbf{w}}, \ \mathbf{w} \in \mathbb{R}^{|H|k}. \tag{15}$$

This relaxation was used in various computer vision fields [24, 25, 26, 27], and a probabilistic interpretation was first proposed by Zass and Shashua [28] and then extended by Chertok and Keller [29].

The r.h.s. of Eq. 15 is a Rayleigh quotient, and thus, $\mathbf{w}^*$ can be computed as the eigenvector corresponding to the leading eigenvalue of $\mathbf{A}$. The binary assignment vector $\mathbf{v}^*$ is computed by applying a discretization procedure to $\mathbf{w}^*$ maximizing the sum of the chosen entries in the vector $\mathbf{w}^*$. This was shown in [29] to correspond to the maximum likelihood inference of the assignments, under an implicit probabilistic model. As there are no assignment constraints, we apply a greedy discretization scheme, where the relaxed assignment vector $\mathbf{w} \in \mathbb{R}^{|H|k}$ is reshaped as an assignment matrix $\mathbf{W} \in \mathbb{R}^{|H| \times k}$. Thus, each row of $\mathbf{W}$ corresponds to the assignments of the set of patches $\widehat{p}_{i,j}$ to a particular pixel $\mathbf{x}_{i,j} \in H$, and we choose the assignment corresponding to the maximal entry in the corresponding row of $\mathbf{W}$.

3.2 Multiscale formulation

We extend the proposed scheme by deriving a multiscale inpainting scheme, using a Gaussian pyramid of images $I_0, I_1, ..., I_m$. The inpainting is applied at the coarsest scale I_m, and the recovered patches h_m are

used as anchors in the inpainting of I_{m-1}. The patches in I_{m-1} whose centers correspond to the locations of h_m are added to the set ∂H_{m-1}, that is the set of embedding constraints in scale $m-1$. This approach is depicted in Fig. 5, where the lower resolution scale is shown in Fig. 5a, while the embedding at the higher scale (Fig. 5b) utilizes the grid-like anchor embedding points computed in the lower resolution scale.

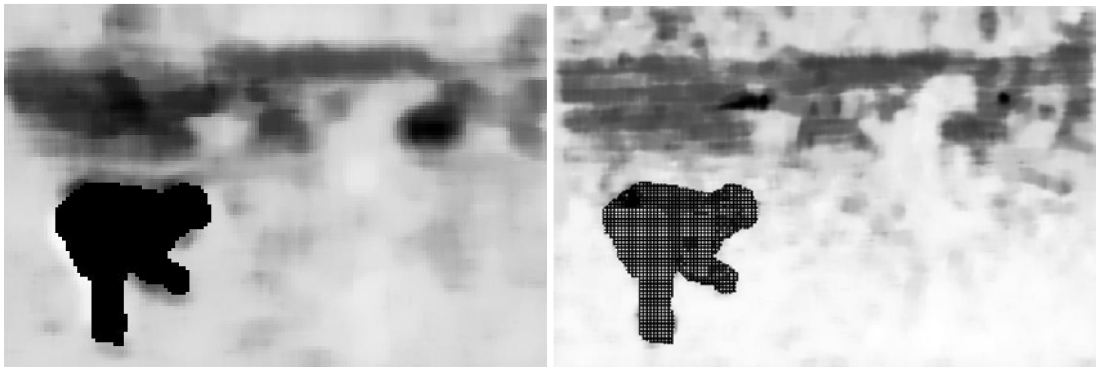

(a) (b)

Figure 5: Diffusion embedding at multiple image resolution scales. (a) Embedding eigenvector of lower scale image. (b) The embedding eigenvectors of a high resolution image replica.

3.3 Affinity measures

In order to achieve a suitable Diffusion embedding as discussed in Section 2.2, one has to choose an appropriate affinity measure to define the Diffusion kernel in Eq. 2. The chosen metric reflects the sort of similarity we are interested in, and the resulting image manifold. For instance, using color descriptors will result in an embedding parameterizing the color manifold of the image. In contrast, in image inpainting we found it most useful to use texture descriptors.

This reflects the relationship between the Diffusion embedding, the heat kernel and the corresponding PDEs. Implying that previous works based on the variational (and PDE-based) formulations, were implicitly operating on an image manifold related to its intensity values. Indeed, such schemes [1] might fail when inpainting textured image regions, and more elaborate schemes that explicitly combine structure and texture inpainting [11] were derived.

We used two texture descriptors: the first being the Local Binary Pattern (LBP) descriptor [23] that characterizes the image texture in the vicinity of each pixel. We use this descriptor to define the

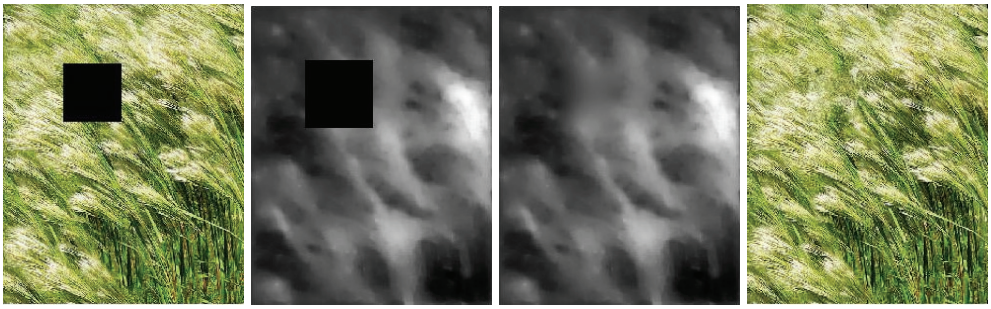

(a) Source image. (b) LBP-based leading eigenvector ψ_1. (c) LBP-based inpainted by isotropic PDE. (d) LBP-based ψ_1 inpainted image.

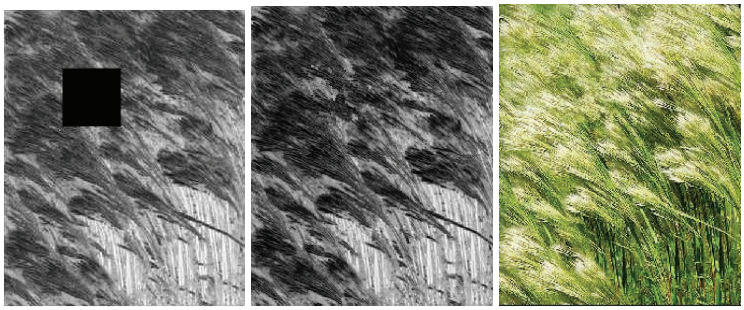

(e) ψ_1 based on the texture descriptor of [7]. (f) ψ_1 based on [7] inpainted by Best-exemplar. (g) Best-exemplar based the result.

Figure 6: Comparing the embedding produced by the LBP and Wexler *et al.*'s [7] texture descriptor. The LBP produces a smoother embedding that can be inpainted using an isotropic PDE, while Wexler's descriptor requires the use of the Best-exemplar [6] for embedding.

similarities between patches in the image. The use of LBP results in a spatially smooth eigenvectors corresponding to the spatial similarity of the image texture. We also used the texture descriptor proposed by Wexler *et al.* [7], consisting of (R,G,B,I_x,I_y), being the color channels and the image intensity gradients. This affinity measure results in a less smooth embedding than the one based on LBP, yet it is smoother than the source image.

We compare the embedding and inpainting results of the two descriptors in Figs. 6b and 6e. The embedding produced by the LBP is smoother than that of Wexler's feature, and while ψ_1 in Fig. 6b can be inpainted using isotropic PDE, the eigenvector in 6e is not as smooth, and we applied the Exemplar-based approach [6]. Figures 6d and 6g show the comparable inpainting results.

Our approach is summarized in Algorithm 1.

Algorithm 1 Image completion

1: **Input**: image I, hole mask $H \subset I$, manifold learning set $\overline{H}$.

2: Compute an image feature for each pixel in $\overline{H}$.

3: Compute the affinity matrix $w_{ij} = \exp(-{d_{ij}}^2/\sigma^2)$.

4: Compute $\Psi\left(\overline{H}\right) = \{\psi_i(\mathbf{x}_{i,j})\}_1^d$ leading eigenvectors of $\mathbf{W}$.

5: Inpaint embeddings $\Psi(H)$ within the hole H.

6: **for all** $x_{ij} \in H$ **do**

7: Search for k-nn points in $\Psi(\overline{H})$: $Z_{i,j} = \left\{\mathbf{y}_{i,j}^1, ..., \mathbf{y}_{i,j}^K\right\} \in \mathbb{R}^d$, and corresponding patches $\widehat{p}_{i,j} = \left\{\mathbf{p}_{i,j}^1, ..., \mathbf{p}_{i,j}^K\right\}$.

8: **end for**

9: Solve the inverse Diffusion mapping using spectral relaxation.

10: Compose the result image by blending the chosen patches.

3.4 Discussion

The proposed scheme relates to variational approaches, as it utilizes the induced smoothness of the image embedding. By choosing different affinity measures (and image descriptors) we can formulate the inpainting process with respect to different image manifolds, such as texture, color and edges. Previous variational schemes were implicitly restricted to using the intensely or color manifold of the image. Thus, our approach allows to apply variational schemes on generalized manifolds such as textured images. In a broader view, the proposed scheme can be applied to the interpolation of generalized signals and datasets, by choosing appropriate affinity measures. For instance, it can be applied to inpainting/interpolating tabular data, where contemporary variational schemes are inapplicable. Initial results of this approach were presented by Liberti et. al. [30].

In contrast, exemplar based schemes forgo the smoothness property of the manifold, and even the assumption that a manifold exists, by inpainting using the nearest neighbor sample. Thus, such schemes are able to inpaint textured ('high dimensional') image regions and tabular data. The downside is that they can only be applied locally, causing the loss of the global optimality of the inpainting. This is exemplified by the propagation of errors in early exemplar based schemes, that was solved by the detection of large scale image structures [6] and iterative approaches [7].

The assumption of manifolds smoothness and low dimensionality is also related to the sparse representations schemes that were applied to image inpainting [21, 22], where the image was represented by a set of patches, approximated by a sparse set of coefficients and a corresponding sparse dictionary. It is interesting to note that both approaches utilize the notion of low-dimensionality manifested by the small number of coefficients and dictionary atoms/eigenvectors used to represent the data. They differ on their approach for deriving the low dimensional representation. While the sparse representation approach explicitly aims for the sparse representation using L_1 minimization, the Diffusion approach assumes the data is low dimensional and recovers the corresponding low dimensional parametrization.

Complexity-wise, our scheme requires a single computation of the distances between the patches in the learning set $\overline{H}$ to compute the Diffusion embedding. The upside is that this computation is conducted as a preprocessing step, while in exampler based schemes such as the Best-exampler and Wexler's work, the distances between the active set of patches and the learning set are computed in each iteration.

4 Experimental results

In this Section we detail the experimental results exemplifying the proposed inpainting scheme. We applied our schemes to real images used in previous works. In Section 4.1 we show the diffusion domain inpainting results using an isotropic heat equation (IHE), while the results of applying the best-exemplar in the diffusion domain inpainting are shown in Section 4.2. Failure cases are presented and discussed in Section 4.3, while implementation and timing details are presented in Section 4.4.

In all examples, the proposed schemes was implemented using a Gaussian kernel, and $K = 10$ candidate patches used as input to the combinatorial solver. We compared against state-of-the-art inpainting schemes. These include Criminisi *et al.*'s Best exemplar[1] [6], the PDE based approach of Tschumperle [4] [2] (using 200 iterations and the default values of the other parameters) and Darren Lafreniere's implementation[3] of Komodakis *et al.*' approach [20] (using the 'full' mode that provides improved inpainting quality). Where possible, we applied these approaches and ours to the images used by Wexler *et al* [7]. Last we inpainted the images using the IHE in the image domain. This emphasizes the benefits of

[1] Available at: http://www.cc.gatech.edu/~sooraj/inpainting/

[2] Available at: http://gmic.sourceforge.net/

[3] Available at: http://www.lafarren.com/image-completer/

operating in the Diffusion domain, that is the focal point of our work.

We are unaware of an objective quality metric for quantifying image inpainting results. Hence, the inpainting quality assessments made in this section are in essence subjective, but we did our best to be as impartial as possible.

4.1 Isotropic heat equation inpainting in the Diffusion domain

In this section we report the results of applying our approach using IHE inpainting in the diffusion domain. For that we implemented an isotropic heat equation solver that was applied to inpaint the embedding vectors which are missing the same domain H as the image.

Figures 7 and 8 shows two examples of inpainting using the LBP as a texture feature, where the features were computed using 15×15 histograms of the pointwise LBP measure [23]. Although the source images (Fig. 8 in particular) are textured, the embedding vectors (Figs. 7b and 8b) are smooth, and are well inpainted by a simple IHE scheme. In contrast, when applying the IHE and the PDE-based scheme of Tschumperle [4] in the image domain, both struggle to inpaint the two images, resulting in over-smoothing in Figs. 7d and 8d. Figures 8d and 8g show that PDE based schemes are able to inpaint narrow objects such as cracks or cables, where the over-smoothing is less evident. The proposed scheme seems to provide the best inpainting results in Fig. 7, while being as good as the Best exemplar in Fig. 8.

We exemplify the effect of varying the number of candidate patches in Fig. 9 for $K = \{1,2,3,5,10,20\}$. Setting $K = 1$ (Fig. 9a) implies that the most similar patch in terms of diffusion distance is used, but no spatial image smoothness is induced. As K increases, the quality of the inpainting improves, as depicted in Figs. 9b-9e. In assignment problems where the number of possible assignments $K > 10$, the performance of the spectral approach (Section 3.1) deteriorates thus reducing the inpainting quality as depicted in Fig. 9f for $K = 20$.

4.2 Diffusion domain inpainting using the best-exemplar

In this section we apply Criminisi's Best exemplar inpainting approach in the Diffusion domain, and show it provides improved results compared to its (common) use in the spatial domain. Figures 10-12 present inpainting results, where we used Wexler's five-dimensional image feature [7], instead of the

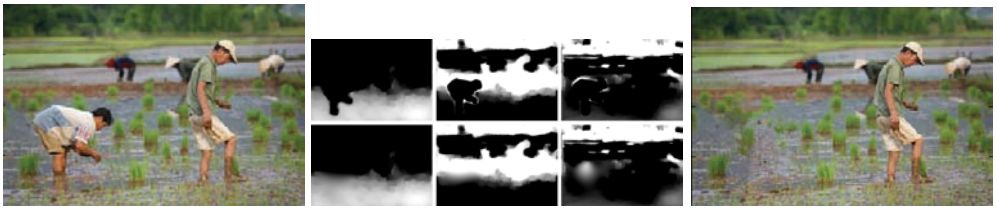

(a) Original (b) The leading eigenvectors and their inpaintings (c) Proposed scheme

(d) Tschumperle et. al. [17] (e) Best exemplar [6] (f) Komodakis et al. [20]

(g) Isotropic heat equation

Figure 7: The inpainting results of the *Rice* image. The embedding was computed using the LBP texture descriptor. The upper row in (b) shows the leading embedding eigenvectors with the unknown part H. The lower row shows the inpainted eigenvectors.

LBP, and the best-exemplar rather than the IHE to inpaint the eigenvectors. In Fig. 10 the proposed scheme proved superior to the other approaches, while in Figs. 11 and 12 our results are on par with those of the Best exemplar and Komodakis *et al.* . These examples emphasize the attributes of the different schemes. In Fig. 10 the unknown region has a global structure that is best inpainted by a globally optimal scheme such as ours. In contrast, the missing region in Figs. 11 and 12 is made of isotropic texture that does not require global optimization, and is thus well inpainted by all schemes. The embedding smoothness is particularly evident in Fig. 12.

In Fig. 13 we show another example of an image combining texture with global structures, that are the dark lines. As in Fig. 10, The proposed schemes provides the best inpainting results as it is able to combine texture synthesis with global optimization. In Fig. 13b we show the three leading embedding eigenvectors, that are the first three Diffusion coordinates of each pixel. It follows, that

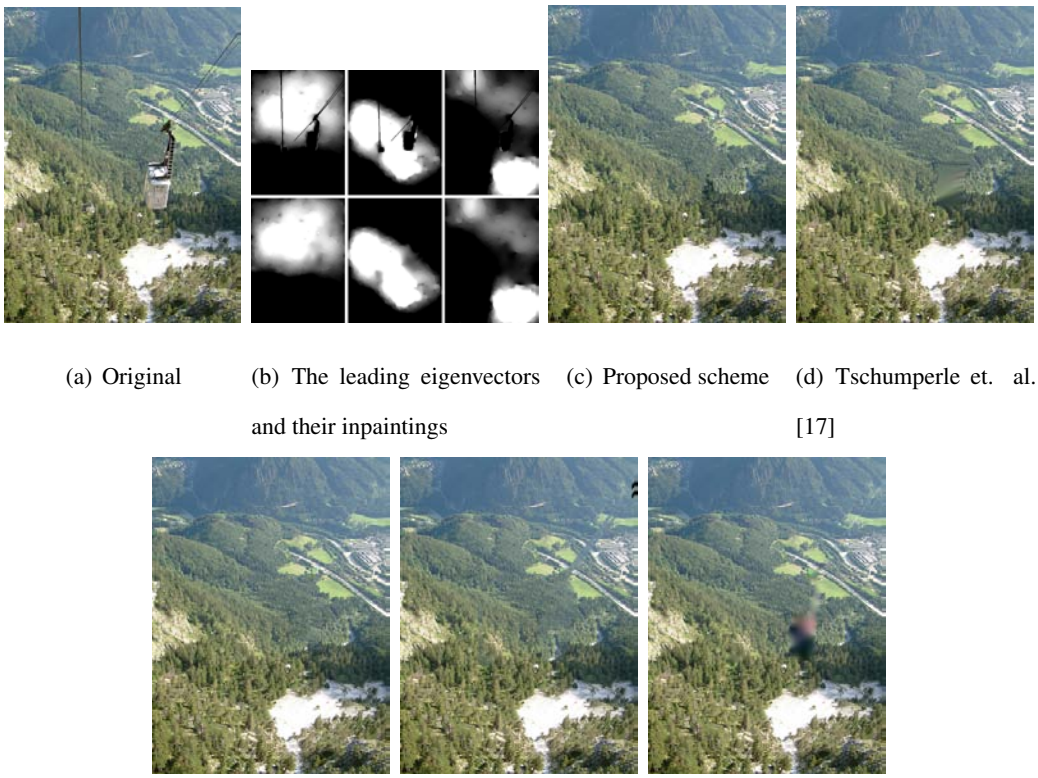

(a) Original (b) The leading eigenvectors and their inpaintings (c) Proposed scheme (d) Tschumperle et. al. [17]

(e) Best exemplar [6] (f) Komodakis et al. [20] (g) Isotropic heat equation

Figure 8: The inpainting results of the *Cable* image. The embedding was computed using the LBP texture descriptor. The upper row in (b) shows the leading embedding eigenvectors with the unknown part H. The lower row shows the inpainted eigenvectors.

by using texture features, the resulting embedding is smooth, making the inpainting easier. Indeed, applying the Best-exemplar in the embedding domain yields improved results compared the applying it in the spatial domain. In Fig. 13c we depict the candidate patches and their locations in the image.

We were unable to obtain an implementation of Wexler *et al.*'s scheme [7] to compare against. Hence, we inpainted the *Bungee* image used in [7] and report the results in Fig. 14. We used the five-dimensional texture features used in [7] and inpainted the embeddings using the Best-exemplar. The eigenvectors in Fig. 14b are relatively smooth and are well inpainted. We achieve comparable results to [7], while being superior to the other schemes. Similar to ours, Wexler's algorithm aims for global optimality, by iterating the image inpainting as detailed in Section 2.1, while our algorithm runs a single iteration.

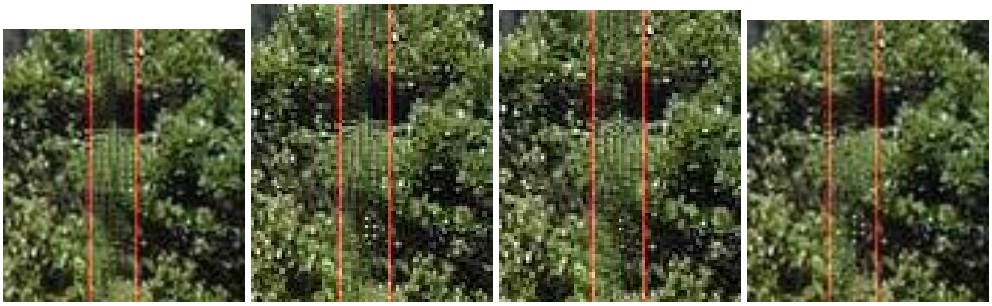

(a) k=1 (b) $K = 2$ (c) $K = 3$ (d) $K = 5$

(e) $K = 10$ (f) $K = 20$

Figure 9: Inpainting result of the proposed scheme with respect to different of K nearest neighbors in the assignment problem (Section 3.1).

4.3 Failure cases

The scheme we propose might fail under certain conditions. We present two such examples in Fig. 15. The first is the *Perrot* image in Figs. 15a-15d. The failure is due to the widening of the unknown regions H in the upper row of Fig. 15. The widening occurs due to the use of 15×15 image patches to define the LBP descriptors. Thus, in order to compute the LBP descriptor on the boundary ∂H, we had to widen H by 30 pixels overall. In contrast, PDE-based schemes use a two-pixels wide boundary ∂H, but might fail to inpaint textured areas. This is depicted in Fig. 15d, where we applied the PDE-based approach of Tschumperle et. al. [17]. Although the inpainting has no artifacts, close visual inspection reveals that the inpainted parts are over-smoothed and that texture details are lost. The second example is shown in Figs. 15d-15f, where the LBP descriptors fail to correctly characterize the image texture. This is evident in the embedding of the first eigenvector in Figs. 15e.

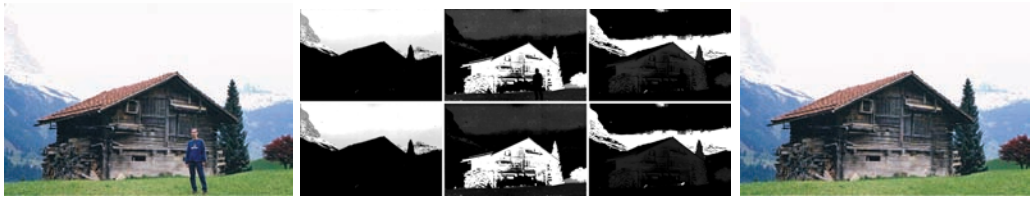

(a) Original (b) The leading embedding eigenvectors and their inpaintings. (c) Proposed scheme

(d) Tschumperle et. al. [17] (e) Best exemplar [6] (f) Komodakis et al. [20] (g) Isotropic heat equation

Figure 10: Image completion using the five-dimensional texture descriptor of [7] and best-exemplar inpainting of the eigenvectors.

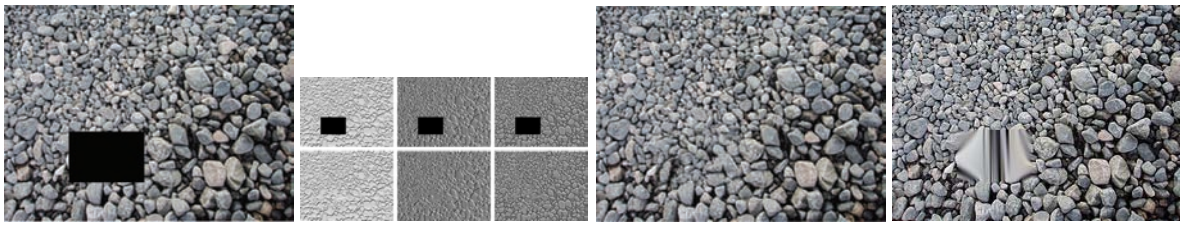

(a) Original (b) The leading embedding eigenvectors and their inpaintings. (c) Proposed scheme (d) Tschumperle et. al. [17]

(e) Best exemplar [6] (f) Komodakis et al. [20] (g) Isotropic heat equation

Figure 11: Image completion using the five-dimensional texture descriptor of [7] and best-exemplar inpainting of the eigenvectors.

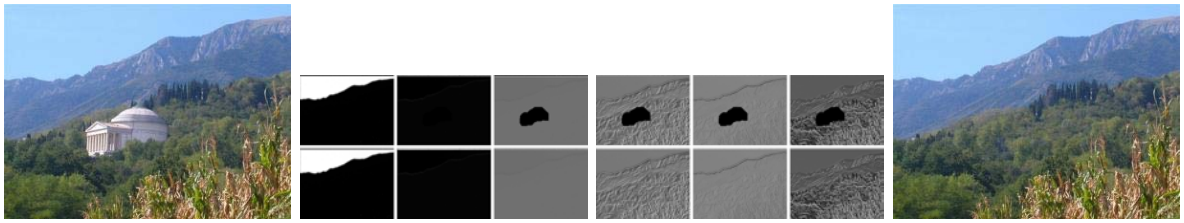

(a) Original (b) Eigenvectors $\psi_1 \div \psi_3$ and their inpaintings. (c) Eigenvectors $\psi_{10} \div \psi_{12}$ and their inpaintings. (d) Proposed scheme

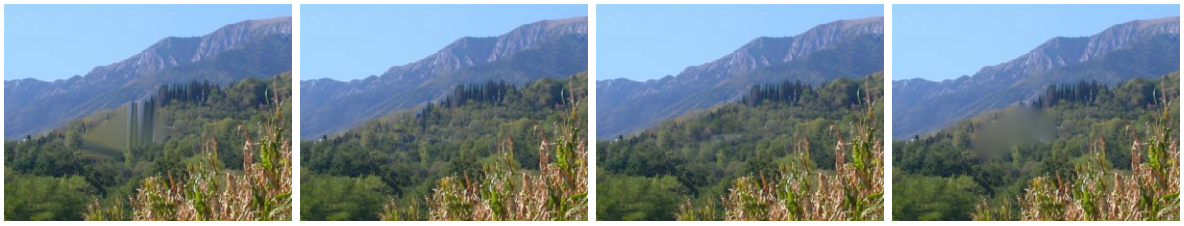

(e) Tschumperle et. al. [17] (f) Best exemplar [6] (g) Komodakis et al. [20] (h) Isotropic heat equation

Figure 12: Image completion using the five-dimensional texture descriptor of [7] and best-exemplar inpainting of the eigenvectors. In (b) and (c) we show some of the embedding eigenvectors. By using the five-dimensional texture descriptor we obtain a smooth embedding.

4.4 Implementation issues

The proposed scheme was implemented in Matlab and the timing was measured on a Quad4-based computer running at 2.6GHz. When inpainting a 200×200 image, the computation of the sparse distance matrix between the LBP features, used to compute the embedding required 11 minutes. Applying the IHE on the Diffusion embedding vectors took a minute, while running the Best-exampler inpainting required three minutes. The approximate inverse mapping using the spectral relaxation lasted three minutes on average. Thus, the overall inpainting takes 15 and 17 minutes, for the IHE and Best Exampler-based schemes, respectively. This timing can be significantly shortened by improving the computation of the patch distance matrix using the Patchmatch approach [16] and its variations.

5 Conclusions

In this work we a proposed a Diffusion based framework for image completion. The crux of our approach is to utilize the Diffusion embedding to induce application specific smoothness over the inpainted image. The induced smoothness is manifested by the smoothness of the embedding eigenvectors, when

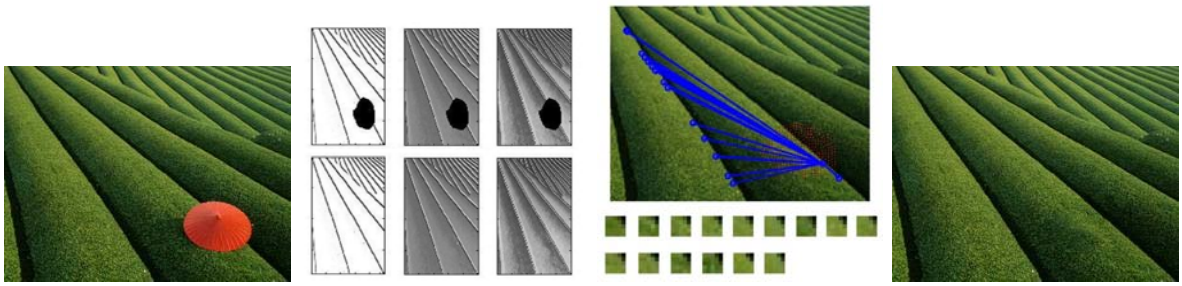

(a) Original (b) The leading embedding eigenvectors and their inpaintings (c) Patch candidates (d) Proposed scheme

(e) Tschumperle et. al. [17] (f) Best exemplar [6] (g) Komodakis et al. [20] (h) Isotropic heat equation

Figure 13: Image completion using the five-dimensional texture descriptor of [7] and Best-exemplar [6] inpainting of the eigenvectors. The three leading eigenvectors are shown in upper row of subplots in (b). Their inpainting using the Best-exemplar approach is shown in the bottom row of subplots. The central pixels of the hole patches are marked by red dots, and the location of the $K = 15$ candidates patches are shown.

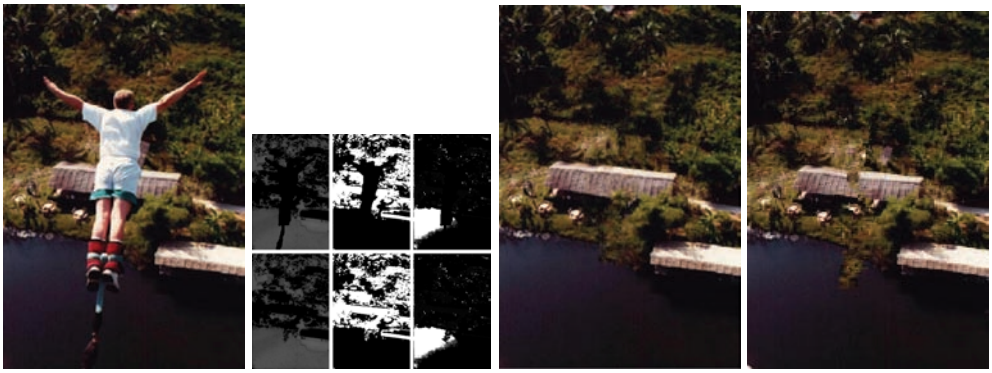

(a) source image (b) The leading embedding eigenvectors and their inpaintings. (c) Proposed scheme (d) Best exemplar result [6]

(e) Wexler et al. result [7] (f) Tschumperle et. al. [17] (g) Komodakis et al. [20]

Figure 14: Inpainting results of the *Bungee* image. The image in (b) was inpainted using a five-dimensional texture feature [7], and Criminisi's Best exemplar inpainting of the embedding vectors.

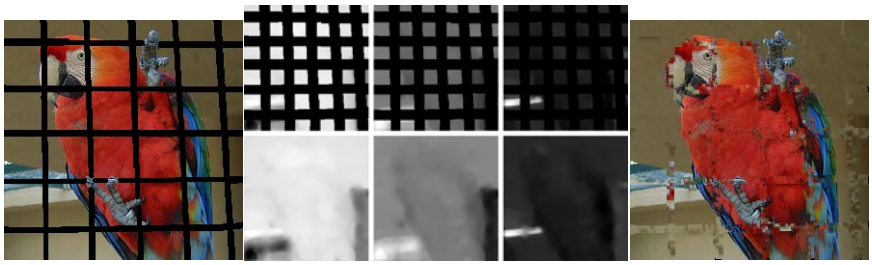

(a) *Parrot* image (b) The leading embedding eigenvectors and their inpaintings. (c) Inpainting results by the proposed scheme

(d) Tschumperle et. al. [17] (e) *Building* image (f) The leading embedding eigenvectors and their inpaintings. (g) Inpainting results by the proposed scheme.

Figure 15: Failure cases.In (d) we show the inpainting by Tschumperle et. al. [17].

computed using appropriate affinity measures, such as the LBP texture features. Thus, we can apply PDE-based inpainting schemes that are commonly only applicable to smooth images, to textured images. In particular, such schemes allow to achieve global inpainting optimality and can be applied to inpainting large-scale holes. We also showed that the use of the Best-exemplar in the diffusion domain, rather than in image intensity domain, yields improved inpainting results. In order to compute an approximate inverse-diffusion mapping, we introduce a novel approach based on discrete optimization, with a corresponding spectral relaxation. The proposed inpainting scheme compares favorably with previous state-of-the-art methods. A major upside of the proposed scheme, is that it can be applied to general datasets such as tabular data, and we reserve that for future work.

References

[1] M. Bertalmio, G. Sapiro, V. Caselles, and C. Ballester, "Image inpainting," in *Proceedings of the 27th annual conference on Computer graphics and interactive techniques*, SIGGRAPH '00, (New York, NY, USA), pp. 417–424, ACM Press/Addison-Wesley Publishing Co., 2000.

[2] M. Bertalmío, "Strong-continuation, contrast-invariant inpainting with a third-order optimal PDE," *IEEE Transactions on Image Processing*, vol. 15, no. 7, pp. 1934–1938, 2006.

[3] J. Shen, S. H. Kang, and T. F. Chan, "Euler's elastica and curvature-based inpainting," *SIAM Journal of Applied Mathematics*, vol. 63, no. 2, pp. 564–592, 2003.

[4] D. Tschumperlé, "Fast anisotropic smoothing of multi-valued images using curvature-preserving pde's," *International Journal of Computer Vision*, vol. 68, no. 1, pp. 65–82, 2006.

[5] A. A. Efros and T. K. Leung, "Texture synthesis by non-parametric sampling," in *ICCV*, pp. 1033–1038, 1999.

[6] A. Criminisi, P. Prez, and K. Toyama, "Region filling and object removal by exemplar-based image inpainting," *IEEE Transactions on Image Processing*, vol. 13, pp. 1200–1212, 2004.

[7] Y. Wexler, E. Shechtman, and M. Irani, "Space-time completion of video," *Pattern Analysis and Machine Intelligence, IEEE Transactions on*, vol. 29, pp. 463 –476, march 2007.

[8] I. Drori, D. Cohen-Or, and H. Yeshurun, "Fragment-based image completion," *ACM Trans. Graph.*, vol. 22, pp. 303–312, July 2003.

[9] J. Hays and A. A. Efros, "Scene completion using millions of photographs," *ACM Trans. Graph.*, vol. 26, July 2007.

[10] J. Mairal, M. Elad, and G. Sapiro, "Sparse representation for color image restoration," *IEEE Transactions on Image Processing*, vol. 17, no. 1, pp. 53–69, 2008.

[11] A. Bugeau, M. Bertalmío, V. Caselles, and G. Sapiro, "A comprehensive framework for image inpainting," *Image Processing, IEEE Transactions on*, vol. 19, pp. 2634 –2645, oct. 2010.

[12] M. Bertalmío, L. A. Vese, G. Sapiro, and S. Osher, "Simultaneous structure and texture image inpainting," in *CVPR (2)*, pp. 707–712, 2003.

[13] R. Coifman and S. Lafon, "Diffusion maps," *Applied and Computational Harmonic Analysis: Special issue on Diffusion Maps and Wavelets*, vol. 22, pp. 5–30, July 2006.

[14] M. Belkin and P. Niyogi, "Laplacian eigenmaps for dimensionality reduction and data representation," *Neural Computation*, vol. 6, pp. 1373–1396, June 2003.

[15] M. Leordeanu and M. Hebert, "A spectral technique for correspondence problems using pairwise constraints," in *International Conference of Computer Vision (ICCV)*, vol. 2, pp. 1482 – 1489, October 2005.

[16] C. Barnes, E. Shechtman, A. Finkelstein, and D. B. Goldman, "Patchmatch: a randomized correspondence algorithm for structural image editing," *ACM Trans. Graph.*, vol. 28, pp. 24:1–24:11, July 2009.

[17] D. Tschumperle and R. Deriche, "Vector-valued image regularization with pdes: a common framework for different applications," *Pattern Analysis and Machine Intelligence, IEEE Transactions on*, vol. 27, pp. 506 –517, april 2005.

[18] S. Masnou and J.-M. Morel, "Level lines based disocclusion," in *ICIP (3)*, pp. 259–263, 1998.

[19] O. Le Meur, J. Gautier, and C. Guillemot, "Examplar-based inpainting based on local geometry," in *ICIP*, (Brussel, Belgique), 2011.

[20] N. Komodakis and G. Tziritas, "Image completion using efficient belief propagation via priority scheduling and dynamic pruning," *Image Processing, IEEE Transactions on*, vol. 16, pp. 2649 –2661, nov. 2007.

[21] J. Mairal, M. Elad, and G. Sapiro, "Sparse representation for color image restoration," *Image Processing, IEEE Transactions on*, vol. 17, pp. 53 –69, jan. 2008.

[22] M. Elad, J.-L. Starck, P. Querre, and D. Donoho, "Simultaneous cartoon and texture image inpainting using morphological component analysis (mca)," *Applied and Computational Harmonic Analysis*, vol. 19, no. 3, pp. 340 – 358, 2005. Computational Harmonic Analysis - Part 1.

[23] T. Ojala, M. Pietikäinen, and T. Mäenpää, "Multiresolution gray-scale and rotation invariant texture classification with local binary patterns," *IEEE Trans. Pattern Anal. Mach. Intell.*, vol. 24, no. 7, pp. 971–987, 2002.

[24] J. Shi and J. Malik, "Normalized cuts and image segmentation," *Pattern Analysis and Machine Intelligence, IEEE Transactions on*, vol. 22, no. 8, pp. 888–905, 2000.

[25] M. Leordeanu and M. Hebert, "A spectral technique for correspondence problems using pairwise constraints," in *ICCV*, vol. 2, pp. 1482 – 1489, 2005.

[26] A. Egozi, Y. Keller, and H. Guterman, "Improving shape retrieval by spectral matching and meta similarity," *Image Processing, IEEE Transactions on*, vol. 19, pp. 1319 –1327, may 2010.

[27] M. Chertok and Y. Keller, "Spectral symmetry analysis," *IEEE Transactions on Pattern Analysis and Machine Intelligence*, vol. 32, no. 7, pp. 1227–1238, 2010.

[28] R. Zass and A. Shashua, "Probabilistic graph and hypergraph matching," in *Computer Vision and Pattern Recognition, 2008. CVPR 2008. IEEE Conference on*, pp. 1–8, June 2008.

[29] M. Chertok and Y. Keller, "Efficient high order matching," *IEEE Transactions on Pattern Analysis and Machine Intelligence*, vol. 32, pp. 2205–2215, 2010.

[30] E. Liberty, M. Almagor, S. Zucker, Y. Keller, and R. Coifman, "Scoring psychological questionnaires using geometric harmonics," in *Snowbird Learning workshop*, 2007.